



A quasi two dimensional metallic state of CaHCl driven by La doping studied from first principles theory

Anuroopa Behatha^a, Vineet Kumar Sharma^a, Gummula Shwetha^b,
Kanchana Venkatakrishnan^{a,*}

^a Department of Physics, Indian Institute of Technology Hyderabad, Kandi, 502285 Sangareddy, Telangana, India

^b Materials Physics Division, Materials Science Group, Indira Gandhi Centre for Atomic Research, 603102 Kalpakkam, Tamil Nadu, India

ARTICLE INFO

Keywords:

Optical isotropy in low energy regime
An insulator to metal transition
Quasi two dimensional nature

ABSTRACT

The present study reports the electronic, optical, vibrational properties and doping studies of the alkaline earth hydride-halides (MHX, M = Ca, Sr, Ba and X = Cl, Br, I) for the first time using density functional theory calculations. The structural optimization and vibrational properties are calculated using the plane-wave pseudo-potential method, and the electronic and optical properties are carried out using the full potential linearized augmented plane wave method. Ground state electronic structure properties ensure these compounds to be direct bandgap insulators except for CaHI, which is an indirect bandgap material with the bandgap ranging from 2.3 to 4.0 eV. Our analysis mainly highlight two aspects: (i) optical isotropy in the studied compounds in lower energy region though they are structurally anisotropic, (ii) quasi two dimensional Fermi surfaces driven by insulator to metal transition by La doping in CaHCl (CaHCl: La) along with anisotropic nature of the electrical conductivity, leading to device applications.

1. Introduction

The ternary hydride-halides, MHX (M = Ca, Sr, Ba and X = Cl, Br, I) falls under the category of PbFCl-type layered structure (P_4/nmm), also known as matlockite structure [1,2]. In general, these simple layered structures grab the focus of many scientists because of its various applications such as medical imaging, X-ray storage properties, image plates, scintillating properties, detection and spectroscopy of ionizing radiation [3]. One such series, which is very well studied, among PbFCl-type structures is MFX (M = Ca, Sr, Ba and X = Cl, Br, I). Doping studies in these compounds with rare-earth ions explains X-ray storage properties [4–9]. These studies include Eu activated BaFCl, which acts as a superior phosphor in X-ray intensifying screens [10]. Doping studies of BaFBr, BaFCl with Eu finds its application as image plates [4,5,11]. Apart from doping studies, many structural, vibrational, optical, and properties under pressure for these compounds are also reported [12–16]. Jiang et al. observed, $LiBH_4$ to exhibit the hydrogen storage properties in presence of CaHCl [17]. In this earlier work, CaHCl was being used as a catalyst, which gave better results as compared to $CaCl_2$. Recently, CaHCl is found to be utilized as a thermal battery for the solar power plant [18]. Claudio et al. studied highpressure phase diagram and

superionicity of alkaline earth metal difluorides using first-principles [19]. Such studies all together motivated us to choose the following series.

Alkaline earth metal hydride-halides, MHX (M = Ca, Sr, Ba; X = Cl, Br, I) adopts PbFCl-type tetragonal structure with space group P_4/nmm (129) and has two formula units ($Z = 2$) in their unit cell. These are layered materials consisting of H-M-X-X-M-H layer and the weak bonding existing between neighboring X-layers reflects the plane of cleavage perpendicular to c -axis. From the previous studies, it has been found that actinides as a doping agent resulted in bandgap engineering, leading to tuned optical applications as compared to host material [20, 21].

Metal-insulator transition (MIT) has attracted much attention over the past 40–50 years and led to the development of many theories [22–31] due to its conceptual complexity and wide technological applications in condensed matter physics. The occurrence of MIT might be due to various effects like physical or chemical doping, strain effects, etc. Yoo and Liao [32,33] reported metal to insulator transitions by chemical doping in $RNiO_3$. Similarly, Shinhora et al. [34] observed the transition from insulating to metallic state driven by doping in NiO. A similar transition in a heavy-fermion superconductor, UTe_2 is due to the

* Corresponding author.

E-mail address: kanchana@iith.ac.in (K. Venkatakrishnan).

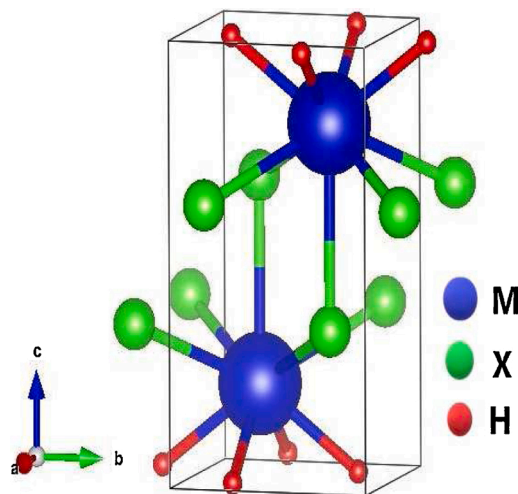


Fig. 1. Crystal structure of MHX (M = Ca, Sr, Ba and X = Cl, Br, I).

inclusion of both Coulomb interaction and spin orbit coupling [35]. These studies further motivated us to proceed with doping analysis in the opted compounds. Hence we present a comprehensive study of mechanical, dynamical, electronic structure, optical and vibrational properties of layered PbFCl type compounds, MHX (M = Ca, Sr, Ba and X = Cl, Br, I) using first principles which are not reported so far. In addition, partial doping of La on Ca site is also analyzed from various perspectives.

2. Computational details

First-principles investigation have been carried out employing a plane-wave pseudopotential method using CASTEP [36,37] and full potential linear augmented plane wave method (FP-LAPW) using WEIN2k [38]. We have performed volume optimization for all these alkaline earth metal hydride-halides using CASTEP. Since these are layered structures, we have included van der Waal's interactions using semiempirical dispersion correction methods (DFT-D) [39–45] in order to match the experimental lattice parameters.

In the present paper, we have analyzed the structural and vibrational properties with a Norm-conserving potentials (which represents the interaction of electrons with ion cores) [46] and a k-mesh of $8 \times 8 \times 4$, $6 \times 6 \times 4$ is used for CaHX (X = Cl, Br, I) and MHX, (M = Sr, Ba; X = Cl, Br, I) respectively under Monkhorst–Pack [47] scheme to sample the Brillouin zone. The initial atomic positions along with the unit cell parameters were relaxed using BFGS-algorithm [48] with the total energy tolerance of 10^{-5} Ry and atomic force tolerance of 0.03 eV/Å. Elastic tensor analysis has been performed in order to check the mechanical stability of these compounds. Dynamical stability has been calculated using DFPT method implemented in VASP [49–52] with a combination of phonopy code [53]

Further electronic and optical properties were calculated by solving Kohn–Sham equations using full potential linearized augmented plane wave method (FP-LAPW) as implemented in WIEN2K code [38]. The exchange correlation effects were treated using generalized gradient approximation (GGA) within the parametrization of Perdew–Burke–Ernzerhof (PBE) [54]. For self-consistent calculations, we took $R_{MT} \times k_{max} = 7$ where R_{MT} is the radius of the muffin-tin sphere and k_{max} is the plane-wave cutoff. For the doping calculations, we have created $2 \times 2 \times 2$ supercell with 48 atoms. Among the 16 Ca atoms, we replaced one Ca atom with one La atom which is equivalent to 6.25% of La doping and two Ca atoms with two La atoms resulting in 12.50% of La doping. Complete structural optimization has been taken care using

Table 1

Comparison between experimental lattice parameters and calculated values.

	Expt. lattice parameters [60]			Present work		
	a(Å)	c(Å)	Volume (Å ³)	a(Å)	c(Å)	Volume (Å)
CaHCl	3.84	6.83	101.03	3.83	6.80	100.19
CaHBr	3.87	7.89	118.38	3.78	7.84	113.57
CaHI	4.02	8.85	143.29	4.04	8.84	144.36
SrHCl	4.11	6.96	117.30	4.12	6.91	117.29
SrHBr	4.23	7.27	129.82	4.21	7.38	130.99
SrHI	4.32	8.38	156.52	4.43	7.65	150.33
BaHCl	4.39	7.24	139.75	4.41	7.19	139.86
BaHBr	4.53	7.39	151.78	4.54	7.33	150.90
BaHI	4.72	7.78	172.93	4.71	7.79	172.96

GGA-PBE functionals employed in VASP [49–52]. We have chosen different doping sites and calculated the ground state energy. Further calculations are carried out for the doping case with minimum ground state energy. The electronic structure calculations are computed with the energy convergence criteria of 10^{-6} Ry and the k-mesh of $4 \times 4 \times 2$ has been chosen in the irreducible Brillouin zone under the Monkhorst–Pack scheme [47]. The optical properties of the doped systems are computed using VASP code. The extraction and plotting of optical properties have been carried out using the post-processing tool named vaspkit [55]. Next, electrical conductivity is calculated using the Boltzmann theory as included in BoltzTraP code [56], within the constant scattering time approximation (CSTA) and rigid band approximation (RBA) [57–59].

3. Results and discussion

3.1. Structural details

Alkaline earth hydride-halides, MHX (M = Ca, Sr, Ba and X = Cl, Br, I) crystallizes in tetragonal symmetry with space group P_4/nmm (129). The experimental atomic positions along with the lattice parameter details were discussed by Von et al. [60]. The crystal structure is shown in Fig. 1 which possess H-M-X-X-M-H layers (where M = Ca, Sr, Ba). MHX series, being layered PbFCl type compounds capture van der Waal's interactions between the layers and are included in the present systems. The details of experimental and calculated lattice parameters are shown in Table 1, and it is evident that the calculated lattice parameters with van der Waal's interactions are in good accord with that reported experimentally.

PbFCl-type of compounds are well known for their tunable optical properties with doping [61–63]. To reduce the bandgap and to find the possible applications, we have proceeded with the doping studies. Among all the 9 compounds which we have discussed, experimental Raman frequencies are available for CaHCl and are in agreement with our results and we have proceeded with CaHCl for the doping calculations. La is selected as a doping element because of its nearly same atomic radii and similar valency as that of Ca atom. As a first step, we have checked the preferred site by replacing La at various sites of Ca and optimized the full structure for both (6.25% and 12.5% La doping) the doping concentrations. Among all, we have selected one configuration for each (6.25%, 12.5%) doping cases based on their minimum energy configuration, possible site preferences and their corresponding energies are shown in Figs. 2 and 3 respectively for 6.25% and 12.5% La-doping cases. The lattice parameters of the optimized CaHCl:La structure are given in the supplementary document (Table 1). We have also calculated formation energy for the two selected doped structure as it is an important criterion to know the stability of the dopant in the host lattice. The formation energy/atom values are found to be -1.106185694 eV (La 6.25%), and -1.16889391 eV (La 12.50%) and these values being negative indicate the structural stability of the structures.

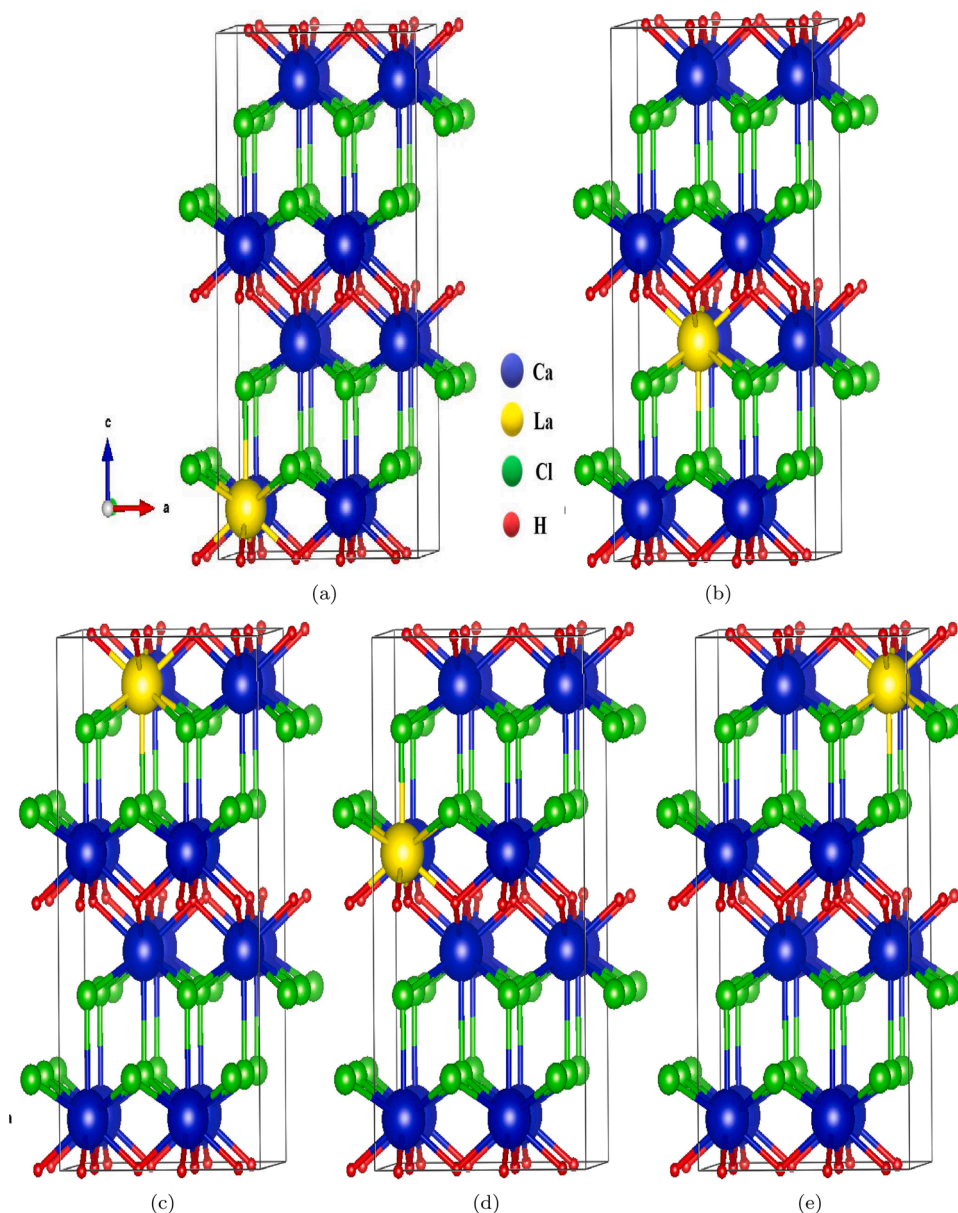


Fig. 2. Site preference energies (in eV) of 6.25% La doping in five different Ca sites: (a) – 192.267, (b) – 191.274, (c) – 196.034, (d) – 191.788, (e) – 195.06

3.2. Mechanical stability

The investigated compounds crystallize in tetragonal symmetry and there exist six independent elastic constants, i.e. C_{11} , C_{12} , C_{13} , C_{33} , C_{44} , C_{66} . The calculated elastic constants are tabulated in Table 2.

From the computed elastic constants, it is vivid that the compounds satisfy the Born stability criteria [64]. Apart from this mechanical stability, other elastic properties like Young's modulus (E), Poisson's ratio (σ), average shear modulus (G), and anisotropy factor (A), etc. are determined from Voigt–Reuss–Hill approximation [65] and the relation linking the elastic constants and the moduli are found elsewhere [66–68]. No experimental studies of elastic properties on these compounds are available so far and needs further verification. Bulk modulus determines the extent to which a substance can resist compression, i.e. hardness depends on the bulk modulus value. Apart from this, shear modulus, G (the ratio of shear stress to shear strain) which is resistant to plastic deformation can also be considered to be a better predictor for

the hardness of a material. Thus from the values of ' B ' and ' G ', CaHCl is considered to be the hardest material in this class of MHX series with the values 43.94 and 25.56 GPa for B and G respectively. The highest Young's moduli, E with a value of 64.23 GPa for CaHCl reflects its stiffness property over other compounds. The value of B/G is an indicator of the ductile or brittle nature of the compound. If $B/G > 1.75$ the compound is ductile or else it is found to be brittle. From Table 2, SrHCl, BaHCl and BaHBr are considered to be ductile. B/G ratio of CaHCl, which is found to be 1.72 (value closer to 1.75) can be considered to be ductile. Poisson's ratio (σ) also confirms this. Since the range of Poisson's ratio for central-force solid is 0.25–0.50 [69], the interatomic forces in the four compounds (i.e. CaHCl, SrHCl, BaHCl, BaHBr) exhibit central-force feature. One more important mechanical property, Debye temperature is also being calculated and it is found that Cl-derivatives possess higher value of θ_D and among all compounds, CaHCl possesses highest value of θ_D .

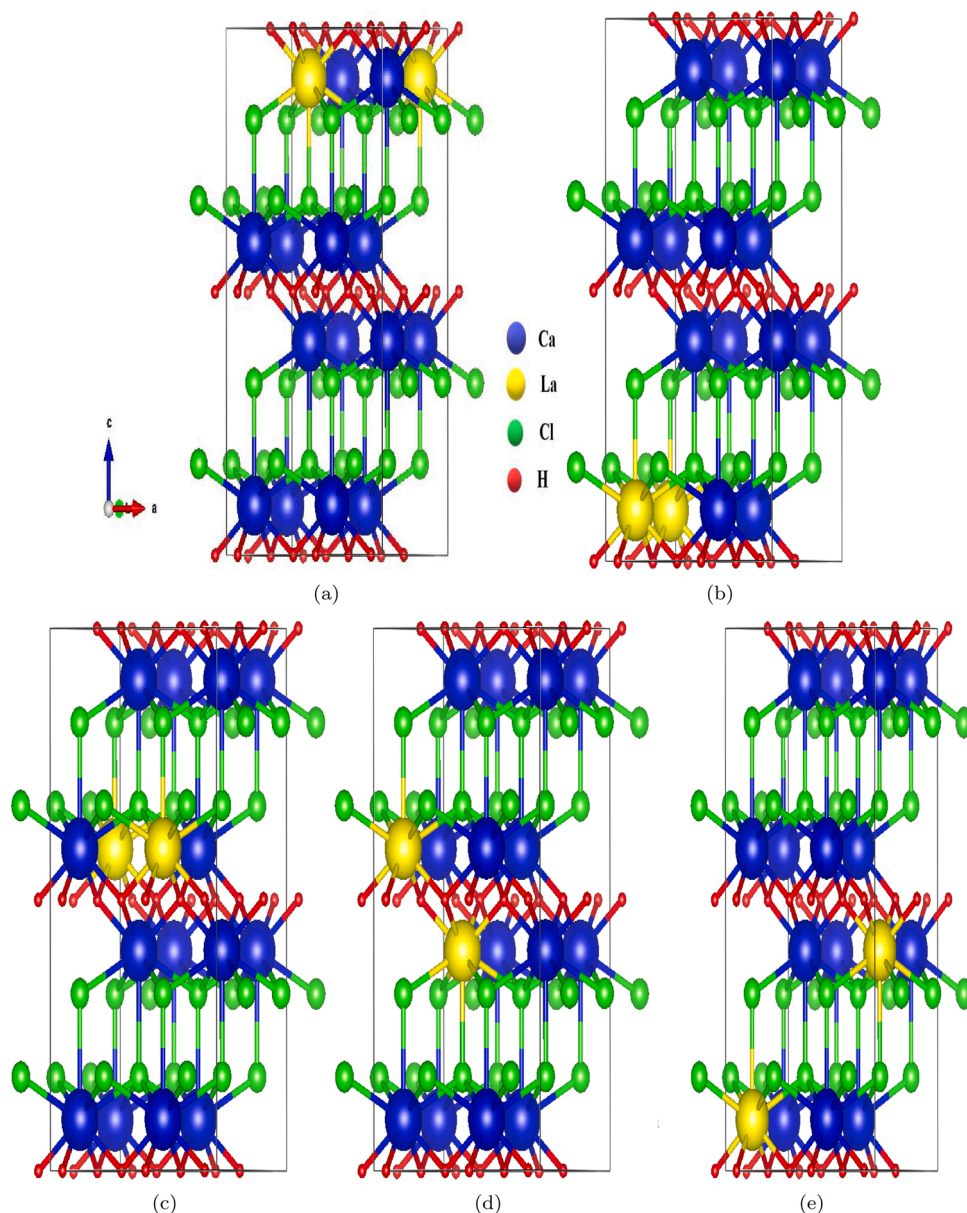


Fig. 3. Site preference energies (in eV) of 12.5% La doping in five different Ca sites: (a) – 197.30, (b) – 194.98, (c) – 202.035, (d) – 187.450, (e) – 191.48.

3.3. Dynamical stability and vibrational analysis

We have computed the phonon dispersion for all the compounds using PHONOPY code. The positive phonon frequencies evidenced in the dispersion plots accounts for the dynamical stability of the system as seen in Fig. 5 and supplementary (Fig. 1). We observe an appreciable phonon gap between high frequency optical and low frequency optical modes. This is due to the huge difference in the atomic masses of H and the other atoms. The high frequency phonon modes are dominated by H atoms. The low frequency optical phonon modes are highly interacting with acoustic modes, and the same are dominated by Ca and Cl atoms. This trend can be understood from the previous work through the relation between atomic mass and phonon frequency [70]. We have plotted the phonon density of states also for better understanding (see in Fig. 5b).

In addition, vibrational properties for all the compounds have been calculated using the linear response method. Group theory analysis which is applied to the tetragonal symmetry (space group P_4/nmm) gives

18 degrees of freedom into modes, which follows the symmetry operations of point group D_{4h} . Also from the structural information available so far, CaHCl consisting of 6 atoms in the primitive unit cell, gives rise to 3 acoustic modes and 15 optical modes at Γ point in the Brillouin zone:

$$\Gamma_{\text{optical(CaHCl)}} = 2A_{1g}(\text{Raman}) + B_{2g}(\text{Raman}) + 6E_g(\text{Raman}) + 4E_u(\text{I.R}) + 2A_u(\text{I.R})$$

where A_{1g}, B_{2g}, E_g are Raman active modes and A_{2u}, E_u are IR active modes. The symbols A and B represents non-degenerate vibrational modes and E denotes the doubly degenerate vibrational modes; with the subscripts 'g' and 'u' representing symmetric and anti-symmetric modes respectively with reference to inversion center. The schematic representation of these modes are presented in Fig. 4 and the computed phonon dispersion of CaHCl is shown in Fig. 5a. Similarly we have computed the Raman spectra for all the compounds (Fig. 5b and supplementary Fig. 2) and details are tabulated in Table 3. Raman spectra of CaHCl is in reasonable accordance with the experimental values

Table 2
Elastic properties of MHX (M = Ca, Sr, Ba and X = Cl, Br, I).

Parameter	CaHCl	CaHBr	CaHI	SrHCl	SrHBr	SrHI	BaHCl	BaHBr	BaHI
C_{11} (GPa)	97.49	94.75	68.64	78.09	65.97	56.61	62.99	57.54	48.75
C_{12} (GPa)	26.07	20.55	12.37	19.23	29.63	17.87	24.59	27.24	26.47
C_{13} (GPa)	35.57	21.58	11.19	30.17	25.27	16.37	23.80	22.73	19.85
C_{33} (GPa)	40.91	24.01	19.91	52.07	47.45	11.22	56.50	51.37	41.22
C_{44} (GPa)	33.66	32.85	20.05	25.69	35.25	24.81	25.16	28.16	27.89
C_{66} (GPa)	33.74	21.20	11.29	25.86	22.66	16.76	15.90	15.24	17.05
B_V (GPa)	47.81	37.88	25.18	40.82	37.75	25.08	36.32	34.65	30.12
B_R (GPa)	40.07	24.17	17.93	40.59	36.62	9.65	36.34	34.60	29.65
G_V (GPa)	29.45	27.33	18.44	24.00	25.23	18.18	20.58	20.54	19.39
G_R (GPa)	21.67	19.32	14.93	22.13	22.18	7.19	19.88	18.85	16.76
B (GPa)	43.94	31.02	21.56	40.71	37.18	17.36	36.33	34.63	29.88
G (GPa)	25.56	23.32	16.69	23.07	23.71	12.69	20.23	19.68	18.08
E (GPa)	64.23	55.96	39.80	58.20	58.66	30.61	51.19	49.67	45.13
B/G	1.72	1.33	1.29	1.76	1.57	1.37	1.79	1.76	1.65
G/B	0.58	0.75	0.77	0.57	0.64	0.73	0.56	0.57	0.60
σ	0.26	0.20	0.19	0.26	0.24	0.21	0.26	0.26	0.25
V_l (km/s)	5.54	4.19	3.36	4.51	4.01	2.76	3.91	3.56	3.25
V_t (km/s)	3.17	2.57	2.07	2.56	2.35	1.68	2.21	2.02	1.88
V_m (km/s)	3.53	2.83	2.29	2.85	2.61	1.86	2.46	2.25	2.09
θ_D (K)	410.92	316.78	236.48	314.94	278.23	185.29	256.75	228.82	203.12

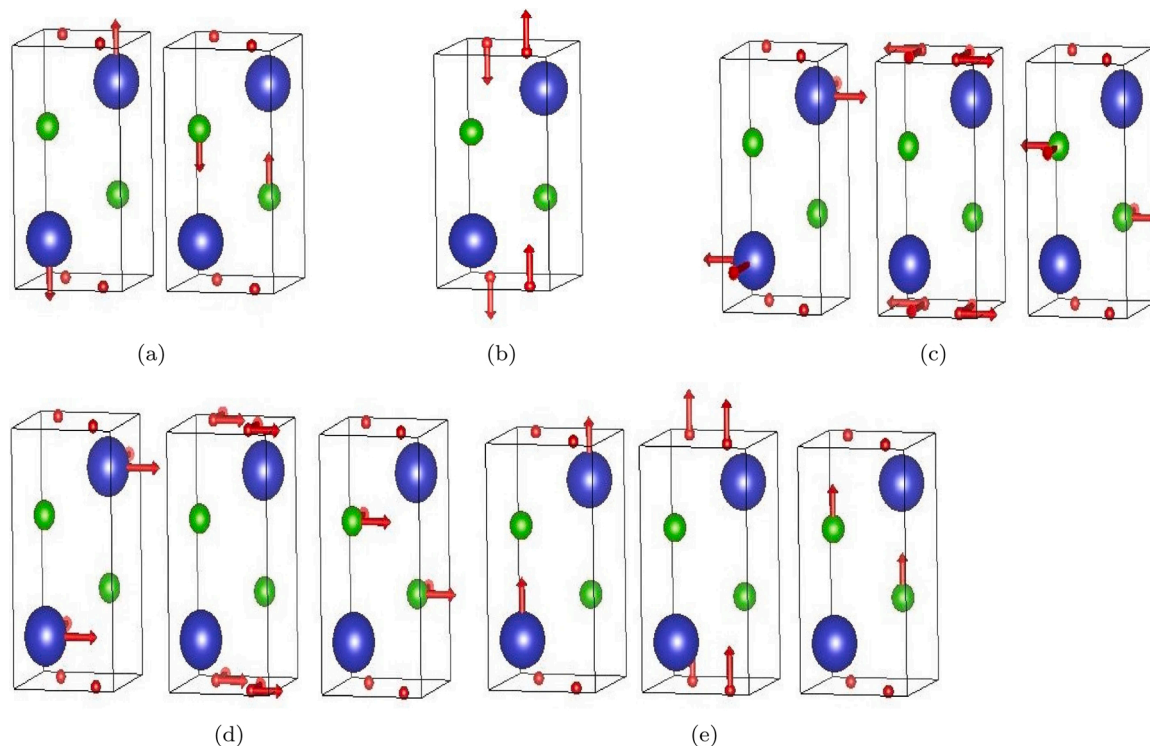


Fig. 4. $2A_{1g}$, $1B_{2g}$, $3E_g$, $3E_u$, $3A_{2u}$ modes of vibration in (a–e) respectively for MHX series. Blue, green, red colors indicate Ca, Cl, and H atoms respectively. (For interpretation of the references to color in this figure legend, the reader is referred to the web version of this article.)

available so far [71].

3.4. Electronic structure details

To interpret the nature of these PbFCl type-layered compounds, we have performed electronic band structure calculations using GGA-PBE [54]. Band structures reveal that, these compounds are insulators with bandgap values ranging from 2.3 to 4.0 eV and these values are given in

Table 4. All the 9 compounds except CaHI possess direct bandgap at 'Z', whereas CaHI has indirect bandgap with valence band maximum (VBM) at 'Z' and Conduction band minimum (CBM) at 'M'. We observe the reduction in the bandgap moving from Cl to I (Cl \rightarrow I). The splitting of valence bands into two manifolds in Cl based compounds (i.e. CaHCl, SrHCl and BaHCl) is attributed to the high electronegativity of Cl among Cl, Br and I (i.e. Cl > Br > I in terms of electronegativity). Electronic band structure of CaHCl is given in Fig. 6a and details of all the

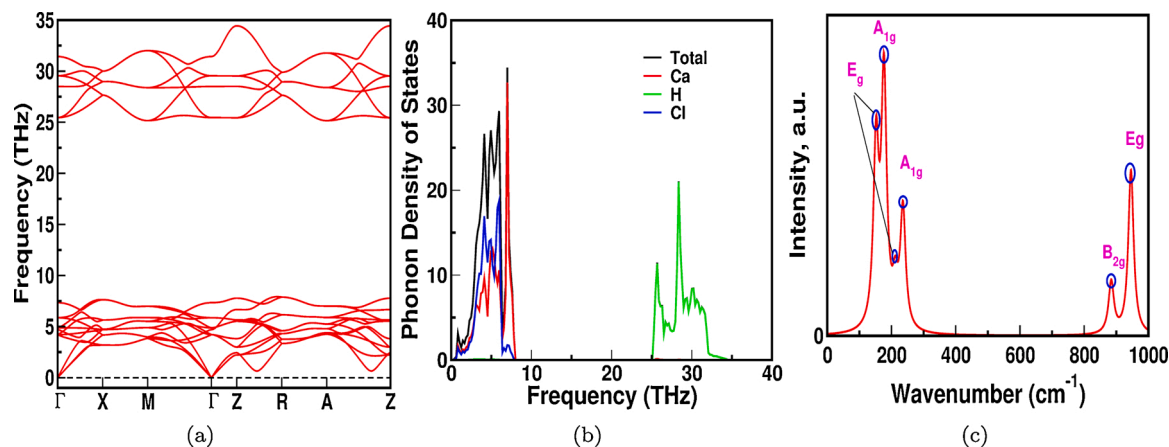


Fig. 5. (a) Phonon dispersion curves of bulk CaHCl along the high symmetry directions indicating the dynamical stability of the compound, (b) phonon density of states, (c) Raman spectra of CaHCl.

Table 3

Details of I.R and Raman frequencies (in cm^{-1}) of MHX (M = Ca, Sr, Ba and X = Cl, Br, I).

	CaHCl	CaHBr	CaHI	SrHCl	SrHBr	SrHI	BaHCl	BaHBr	BaHI
<i>Raman</i>									
A_{1g}	177	103	77	122	86	77	133	110	58
	236	233	191	177	141	124	179	125	89
B_{2g}	884	897	812	843	804	732	685	658	98
E_g	152	78	56	99	82	57	76	66	59
	212	177	149	156	121	109	146	110	101
	946	954	869	875	831	771	735	693	631
<i>I.R. frequencies</i>									
A_{2u}	153	150	129	120	80	87	160	114	83
	996	1014	926	940	899	839	813	773	732
E_u	179	145	111	120	102	94	120	94	86
	738	810	715	773	718	622	619	585	536

Table 4

Calculated bandgap (in eV) of MHX (M = Ca, Sr, Ba and X = Cl, Br, I).

	CaHCl	CaHBr	CaHI	SrHCl	SrHBr	SrHI	BaHCl	BaHBr	BaHI
Bandgap	4.009	3.881	3.195	4.235	3.216	3.202	3.096	2.696	2.306

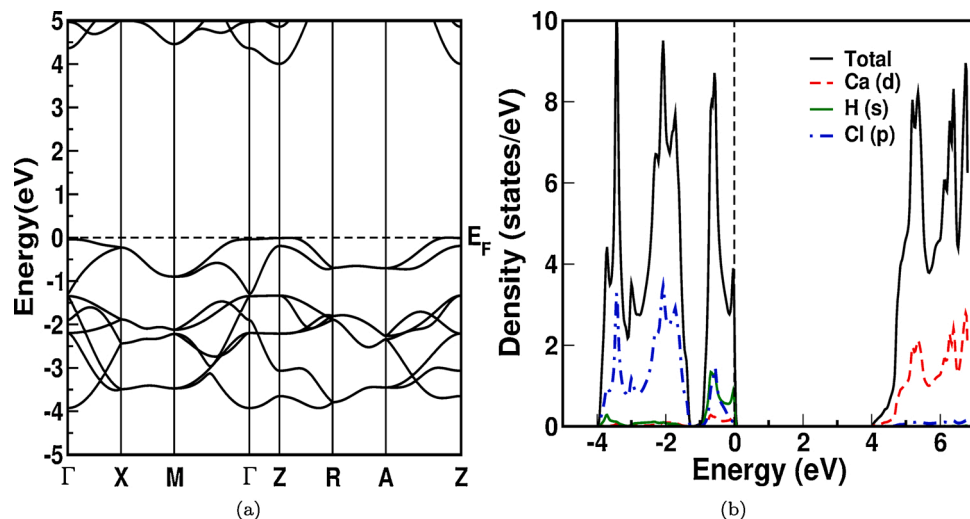


Fig. 6. Bandstructure along with Partial DOS for CaHCl in (a) and (b) respectively.

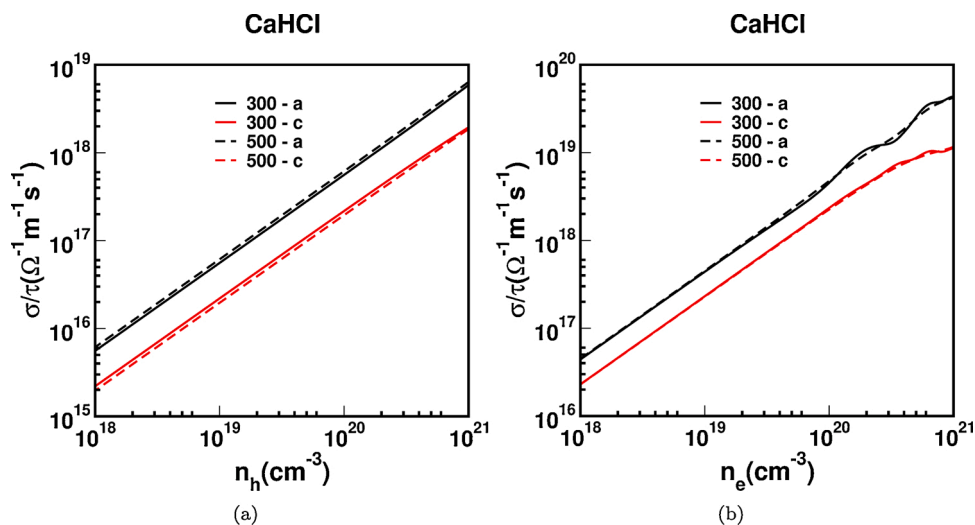


Fig. 7. The electrical conductivity scaled by relaxation time for CaHCl: (a) holes and (b) electrons.

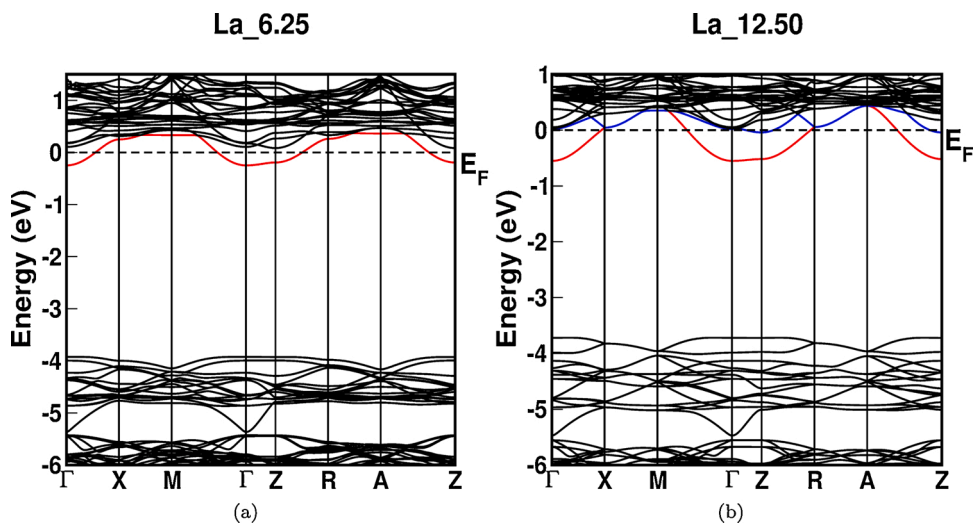


Fig. 8. Band structures of (a) 6.25% La doped (b) 12.50% La doped CaHCl which shows the shifting of the energy level when compared to host.

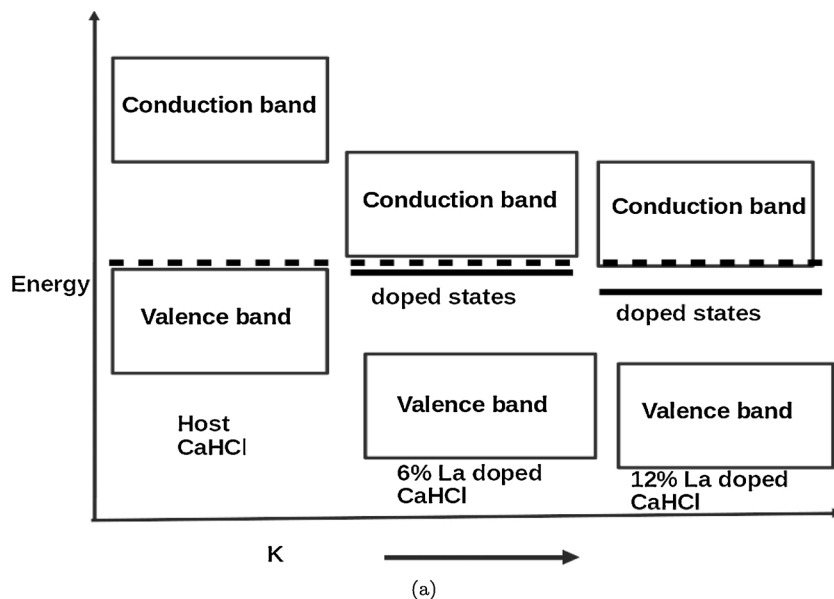


Fig. 9. Schematic diagram showing the relative variation of states compared to host, 6.25% La doped, 12.50% La doped CaHCl indicating insulator to metal transition. Dotted line indicates the Fermi level.

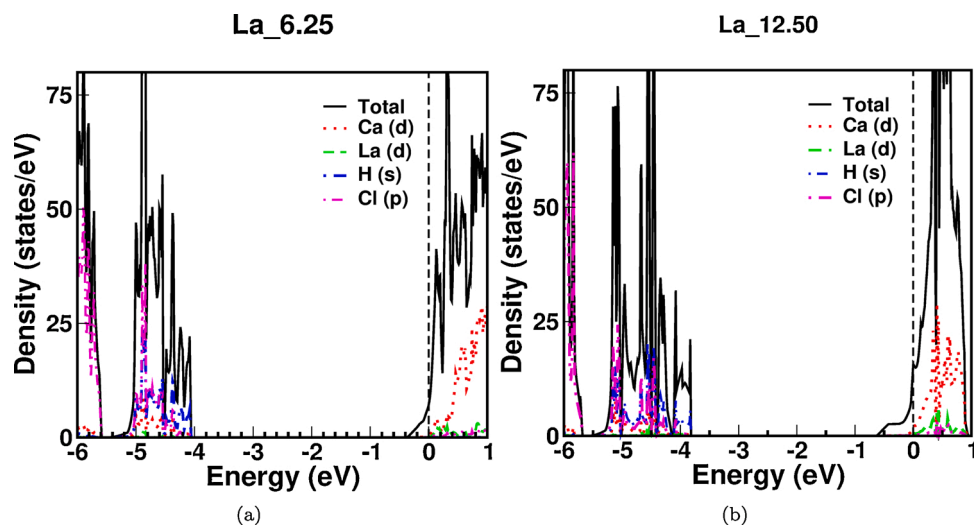


Fig. 10. Density of states of (a) 6.25% La doped, (b) 12.50% La doped CaHCl.

compounds are presented in supplementary (S) (see Fig. 3).

In order to understand the individual atomic contributions close to Fermi level, E_F , we analyze the partial density of states and the details of CaHCl alone is provided in Fig. 6b. The valence band is predominantly due to the hybridization of H-s and Cl-p states, whereas, the conduction bands are due to Ca-d states (i.e. 3d state) in CaHCl. We observe exactly the same trend in all other compounds.

In Cl based compounds, the splitting of valence bands into two manifolds increases as we move from Ca to Ba (i.e. Ca \rightarrow Sr \rightarrow Ba). In valence band, the first manifold shows its predominant H-s with less contribution from Cl-p and M-d (M = Sr, Ba) states and then next manifold at around 2-4 eV arises from Cl-p states, whereas in conduction band, the predominant contribution comes from 3d, 4d, and 5d states of Ca, Sr, Ba respectively. The similar trend is observed in Br and I based compounds as well and the details are provided in supplementary (S) (see Fig. 4). Band dispersion of CaHCl further motivate us to check the anisotropy as the investigated system is tetragonal. We have calculated the electrical conductivity scaled by relaxation time along 'a' and 'c' axes. The anisotropy can be seen from the plots 7 and the value of electrical conductivity scaled by relaxation time along 'a' axis is higher than that of 'c' axis for both the carriers. This nature can be understood from the band structure also. The bands are more dispersive along Γ -X than along Γ -Z in both the conduction and valence band regions. The anisotropy in case of holes is more appreciable than that of electrons and this nature is found to be increased by band engineering as a function of doping.

When it comes to doping, we have optimized the structures and proceeded for the electronic structure and optical properties studies. From the band structure plots (shown in Fig. 8), we can observe that valence band and conduction band states are moving down as a result there is a clear change in the band structure of doped system when compared to the host. Interestingly, we have seen the new states appearing around -0.28 eV for 6.25% La doping and 0.55 eV for 12.5% La doping by crossing the Fermi level, i.e. with La doping the system is driving towards metallicity. The schematic diagram is also shown in Fig. 9 with the relative variation of the doping states compared to the host. In this figure, we can see that new states are dropping down below the Fermi level resulting in insulator to metal transition with La doping. We can also see that these states are still moving to lower energy regions with an increase in the La doping content, i.e. metallic nature is increasing with the increase in La doping. To have a better understanding regarding the states present near the Fermi level, we have plotted the density of states (DOS) for both the cases as seen in Fig. 10. The state near the Fermi level are hybridized 'd' states of La and Ca. The DOS at the Fermi level ($N(E_F)$) increase with the doping percentage

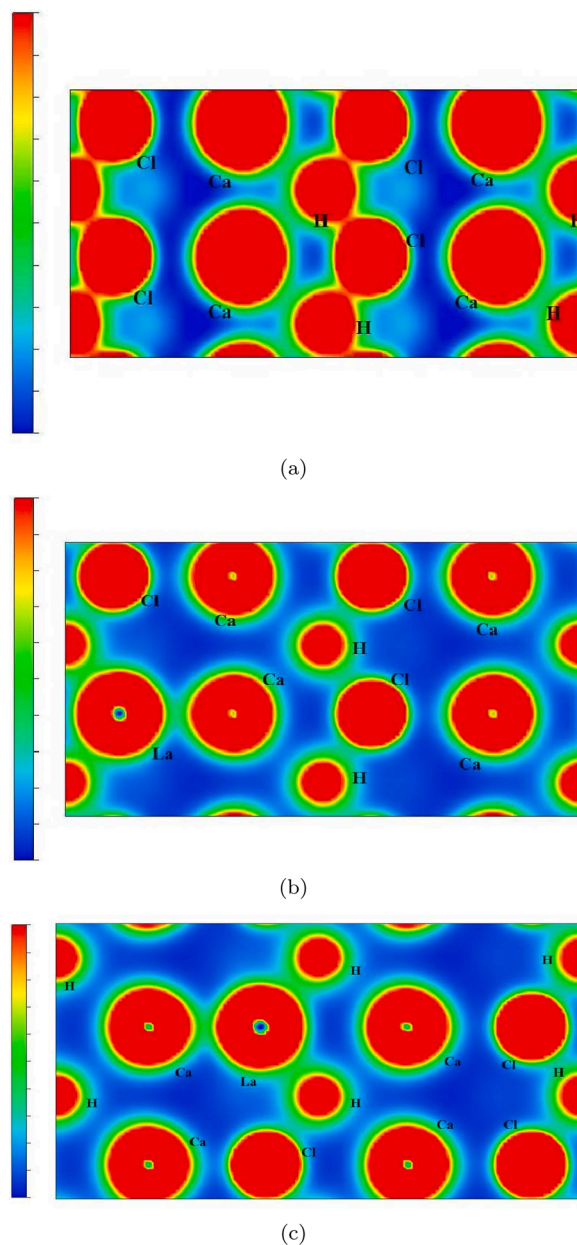


Fig. 11. Charge density plots of (a) host, (b) 6.25% La doped, (c) 12.5% La doped CaHCl in 100 direction.

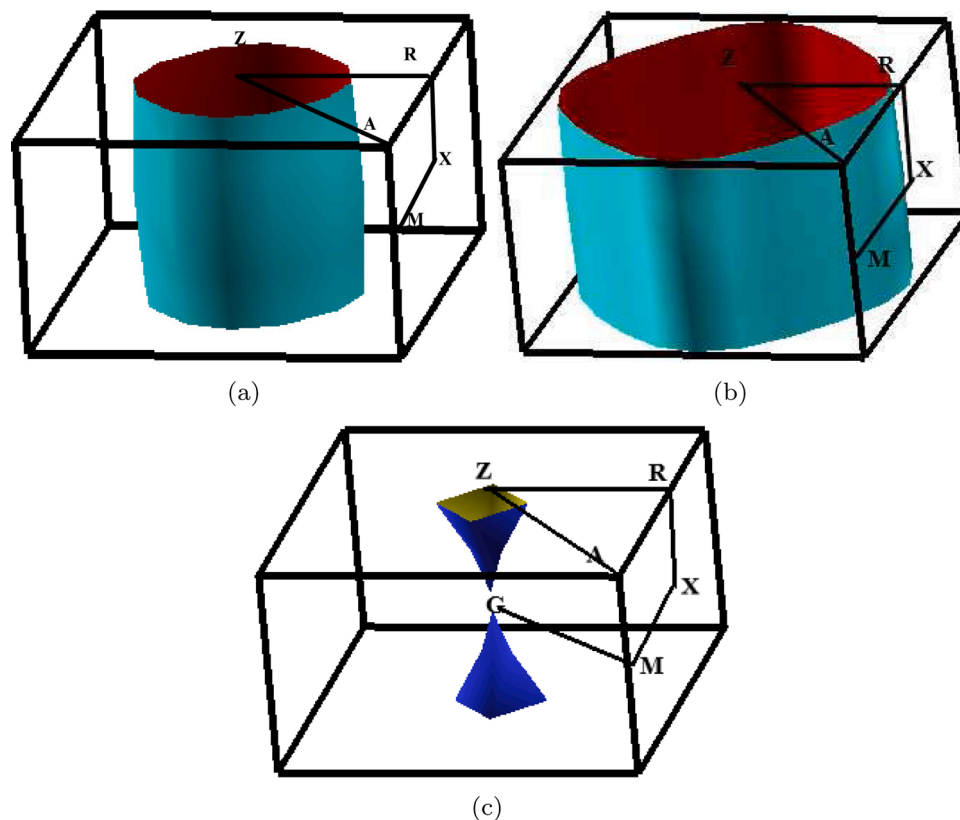


Fig. 12. Fermi surfaces of (a) 6.25% La doped, (b,c) 12.50% La doped CaHCl.

$N(E_F) = 7.4$ states/eV for 6.25% La doping and $N(E_F) = 15.6$ states/eV for 12.5% La doping. DOS plot also clearly shows that due to La doping, additional states are present in the valence bands which indicate that La doping in CaHCl drives it to a metallic state. Similar results are also observed in NaOsO₃ with Mg doping [72]. With the increase in the La doping to 12.5% the lower energy levels of conduction band shifts still lower, driving the system to be more metallic. This prediction is further verified from the optical properties calculations.

To understand the doping effect on host material, we have shown and analyzed the charge density plots for the host, 6.25% La, 12.5% La doped CaHCl with the same cell size as shown in Fig. 11. The red color corresponds to the higher value of charge localized. From the host charge density, we can see covalent nature between Cl-H atoms as they are sharing the charges, and Ca-Cl, Ca-H reveals the ionic nature of the bonds. The host compound is found to have a mixed nature of bonding. Once we move to 6.25% La doping case, we can see that La is forming a covalent bond with Ca which is also confirmed from the DOS plots where one can visualize the hybridization of states between La-*d* and Ca-*d* states. Apart from this, La is also forming a covalent bond with H atom which can be confirmed from the lower energy levels of the valence band in DOS figure. In the case of 12.5% La doped CaHCl, La is forming covalent bond with Ca, H which is also evident from the DOS plot.

Since La doping induces the insulator to quasi 2D metal transition, we have calculated Fermi surfaces in both cases. We found a band crossing E_F in the case of 6.25% La-doped CaHCl, while it is two bands in the case of 12.50% La-doped CaHCl. The Fermi surface corresponding to red colored bands (in Fig. 12(a) and (b)) is cylindrical shaped in both doping cases. This shape can be correlated to the band dispersivity. The dispersion along Γ -X, M- Γ , Z-R, and A-Z are almost the same. This dispersion is responsible for the curved surface of the cylinder centered at Γ point and open surface along Γ -Z. The same is reflected for the

corresponding band in the case of 12.50% doped CaHCl. The second band in the case of 12.50% doped CaHCl is a conical kind of surface with tip (as seen in Fig. 12(c)) towards Γ point and open surface at Z with a rectangular base. This is due to flat band crossing along Γ -Z-R. The band at Z point is completely flat. The computed Fermi surfaces reflects the quasi 2D dimensional nature [73] in the case of La doped CaHCl.

To confirm the quasi 2D dimensional nature in the system, we have calculated electrical conductivity (σ/τ) within the relaxation time approximation along 'a' and 'c' axes for holes with 6.25% doping which is shown in Fig. 13 (a). From the plots, we can observe that the electrical conductivity is independent of carrier concentration and temperature for holes, which can be seen in Fig. 13(a). From the directional dependent analysis, it can be stated that there is a huge anisotropy with an order of 10 in case of holes. Its value is found to be higher along *a* axis when compared to that of *c* axis which is in good accordance with the band dispersions along the respective axes in valence band region. As we increase the amount of doping, its value is shooting up by a factor of 10 along both directions which can be seen in Fig. 13(c). In addition, the σ/τ for electrons are also calculated but these are promising in higher range of concentration (Fig. 13(b) and (d)). The anisotropic nature of the electrical conductivity (σ/τ) is validating the quasi 2D nature of the Fermi surfaces which opens up the channel to explore future device applications.

3.5. Optical properties

The optical properties such as dielectric constant, absorption coefficient and refraction spectra are analyzed for all the nine compounds. As a first step, we computed the complex dielectric function which reflects the behavior of the system towards electromagnetic radiation. The imaginary part, ϵ_2 reflects the optical transition phenomena in the

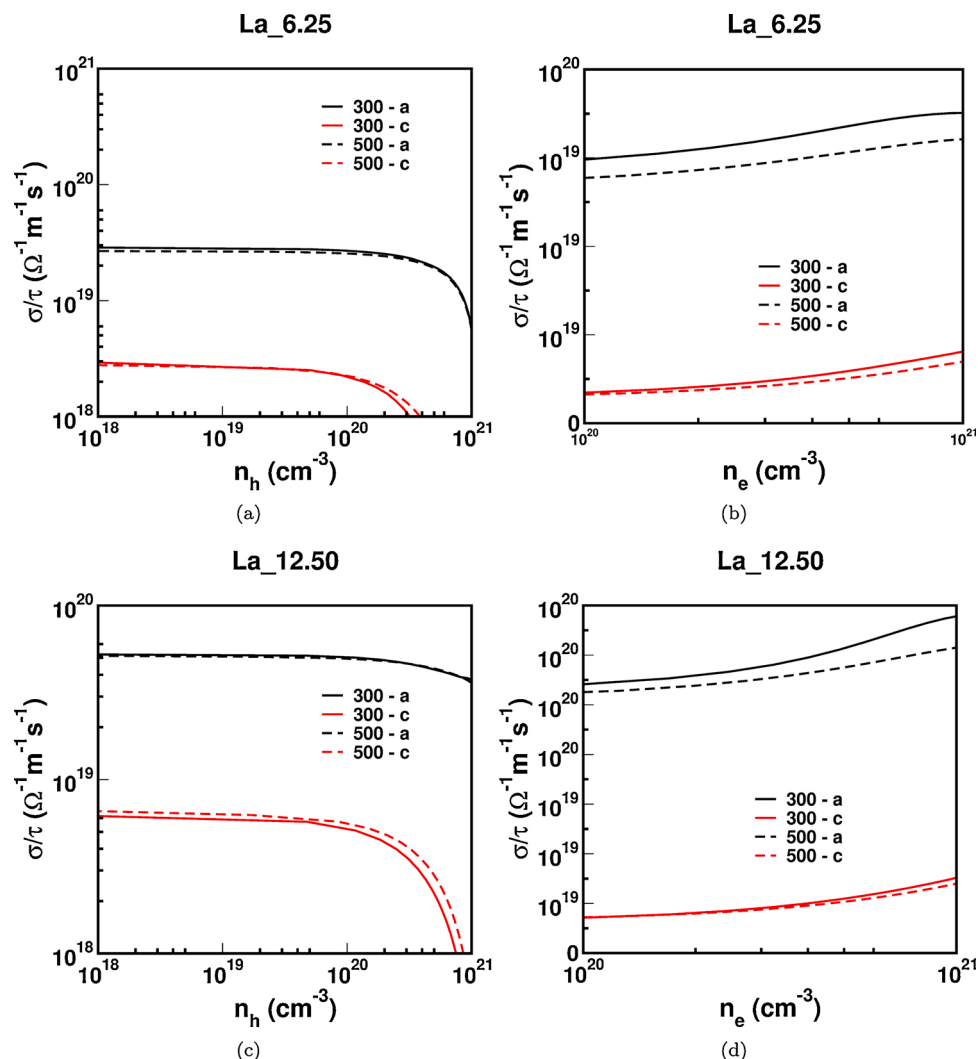


Fig. 13. The electrical conductivity scaled by relaxation time for (a,b) 6.25% La doped, (c,d) 12.50% La doped CaHCl.

electronic band structure and real part, ϵ_1 is obtained from an imaginary part using Kramers–Kronig relation [74].

The peaks in the ϵ_2 of the dielectric function confirm the transition from corresponding valence band to conduction bands. As an example, in CaHCl (see Fig. 14a), we observe the peaks at around 5.6–8 eV, which may reflect the transition from H-s & Cl-p states to Ca-d, very less to Ca-p states and the peaks at around the energy range of 25–27 eV is mainly due to transition from Cl-p to Ca-d states. In the similar manner in all the present compounds under study, we observe the peaks in the imaginary part of dielectric function which may confirm the transition from H-s, X-p (X = Cl, Br, I) states to M-d (M = Ca, Sr, Ba), Ca-p states.

The static dielectric constant is found to follow the opposite trend for bandgap. Accordingly, as we move from Cl → I in all compounds, bandgap decreases, and static dielectric constant increases. This can be observed in the dielectric spectra given in the supplementary document (see Fig. 5(a)–(c)) for Ca based compounds. Similar trend is observed in both Sr-based and Ba-based series which are given in supplementary document (Fig. 5(d)–(f)) and (Fig. 6(g)–(i)) respectively. The onset of curve in ϵ_2 rises from one particular energy called the threshold energy, which is consistent with the band gap of those compounds.

We then calculated the absorption spectra for this series of compounds under study. Absorption spectra describe how material absorbs

the incident electromagnetic radiation. There is no absorption below 4 eV in case of CaHCl (see Fig. 14b) because no transitions are allowed in this energy gap and the material behaves transparent. The absorption starts at 4 eV due to direct transition between H-s & Cl-p states lying in valence bands to Ca-d, Ca-p states lying in conduction bands. The absorption spectra is different in both crystallographic directions due to allowed transitions along both the axes. The absorption is higher along the x-axis in a higher range of energy. Moving down the column of halogens, it is vivid that the absorption spectra shifts towards the lower energy region because of the reduction in bandgap from Cl → I in all the compound and this variation is given in the supplementary document (see Fig. 6).

Further, we have calculated the refractive indices along both crystallographic directions (n_{xx}, n_{zz}). The plot clearly shows optical isotropy predominantly in lower energy region in these series of compounds. The calculated static refractive indices values along x and z-directions are given in Table 5, and these values clearly indicate the isotropic nature in the low energy region. From this table, we can also observe the static refractive indices to follow the increasing trend as we move from Cl → I. This shows that they follow exactly opposite trend in terms of bandgap (i.e. bandgap decreases from Cl → I). It is worth mentioning that the same behavior is observed in BaXF series, (X = Cl, Br, I) [75] and ASrI₃

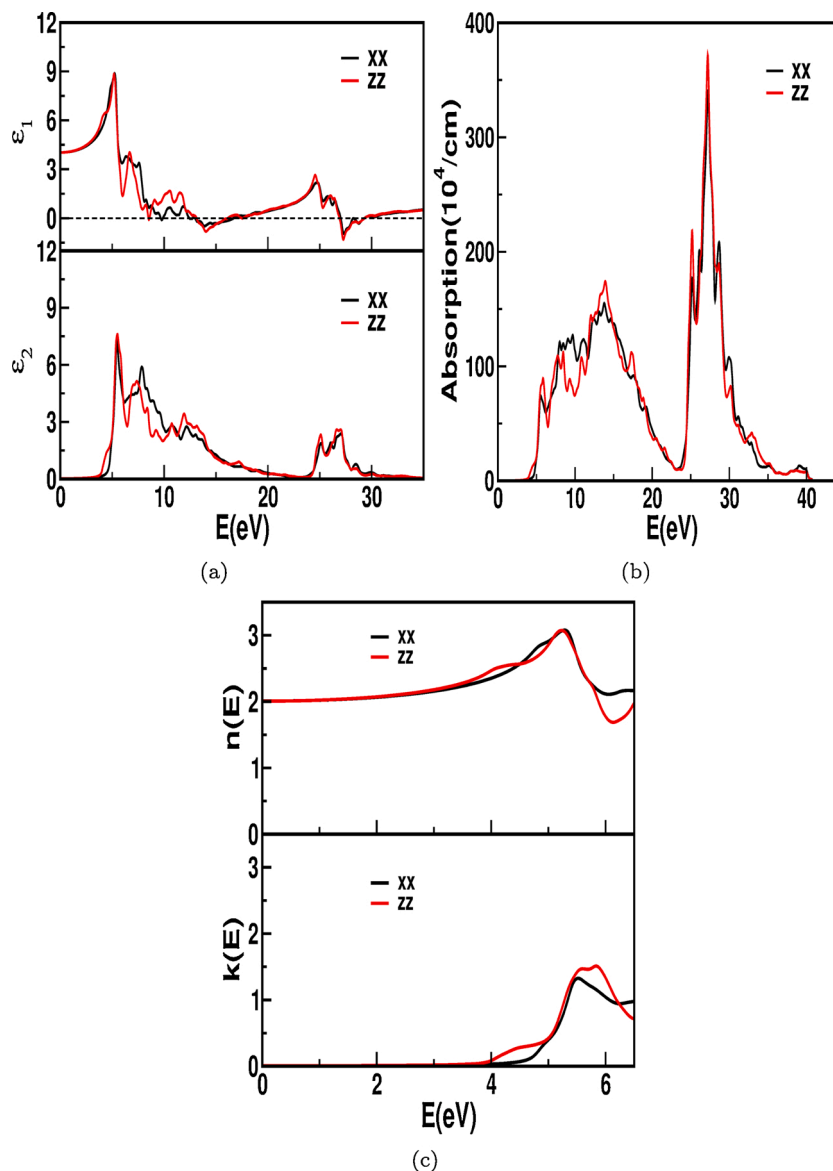


Fig. 14. Dielectric, absorption and refractive spectra of CaHCl in (a–c) respectively.

Table 5

Refractive indices along x and z directions in MHX (M = Ca, Sr, Ba and X = Cl, Br, I).

	CaHCl	CaHBr	CaHI	SrHCl	SrHBr	SrHI	BaHCl	BaHBr	BaHI
n_{xx}	1.98	2.04	2.19	1.94	2.03	2.16	1.91	2.02	2.12
n_{zz}	1.98	2.03	2.16	1.95	2.06	2.19	1.91	2.02	2.12

series [76]. Also, it is very well seen that, these values satisfy the relation $n = \sqrt{\epsilon_r}$ (i.e. $n = \sqrt{\mu_r \epsilon_r}$, where $\mu_r = 1$ for most materials). The variation of the refraction spectra from Cl \rightarrow I is given in the supplementary document (see Fig. 7)

The refractive index spectra as well as the value of static refractive indices (see Table 5) clearly reveal the optical isotropy nature, in all the investigated compounds in the lower energies though the structure is anisotropic.

Similarly the calculated optical properties like absorption spectra and refractive index of 6.25% and 12.5% La doping in CaHCl are shown

in Figs. 15 and 16 respectively along with the host $2 \times 2 \times 2$ supercell. From the absorption coefficient plots (Fig. 15(a) and (b)) of 6.25% La-doped case, we can see small peak which is at the 0.6 eV in the x-direction (0.47 eV in the z direction) revealing the metallicity of the compound which is also seen in 12.5% doped case with increased intensity values, again confirming the increase in metallic nature with increase in the La content. These low energy peaks may be due to the intra-band transition of d–d states. Earlier reports reveal a similar scenario in W doped TiO_2 [77]. The next absorption point which starts around 3.84 eV (3.71 for z-direction) and peaks at 5.56 eV is due to the

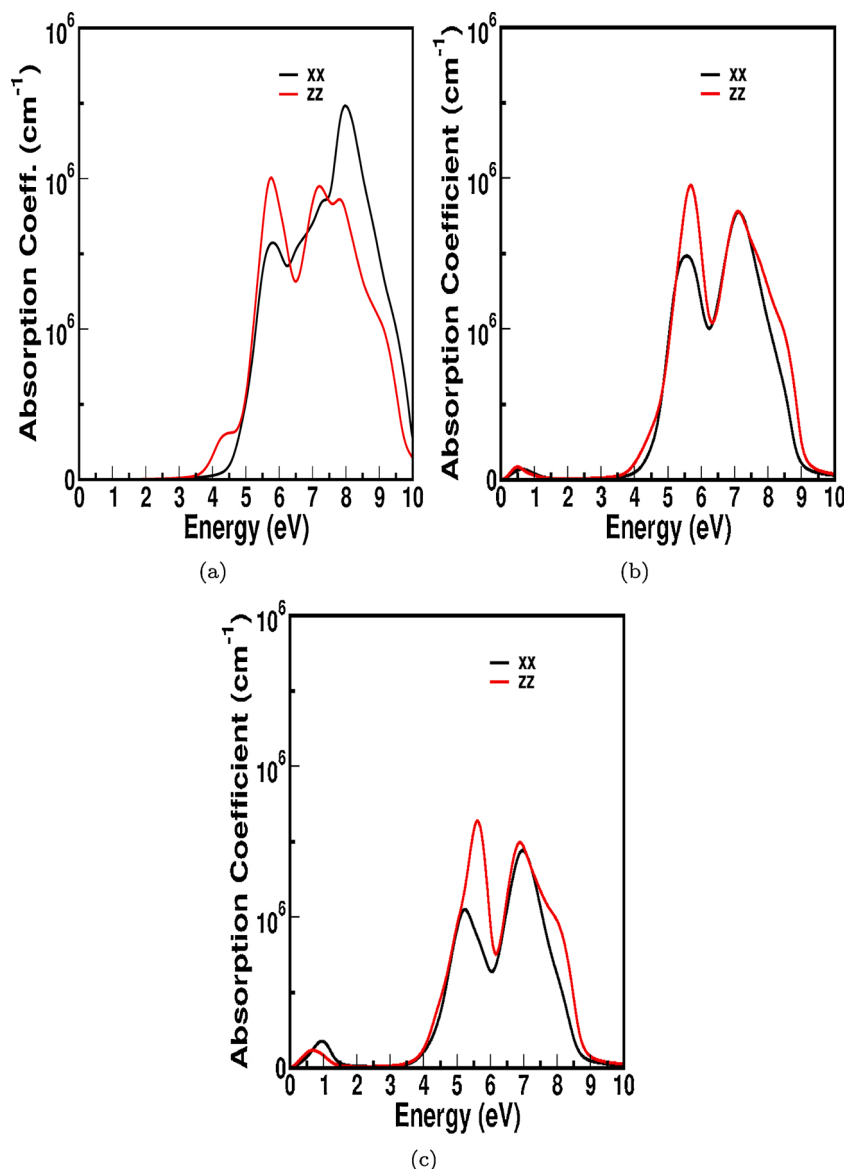


Fig. 15. Calculated absorption spectra of (a) host, (b) 6.25% La doped, (c) 12.5% La doped CaHCl.

transition of H-*s*, Cl-*p* states to La-*d*, Ca-*d*, Ca-*p* states. The peaks in the higher energy is due to the electron transition from the valence band to higher states of the conduction band. In case of 12.5% doping, these transition peaks are observed at 5.26 (5.63), 7.01 (6.9) eV in *x* (*z*)-direction and arises mainly due to electron transfer from H-*s*, Cl-*p* states to La-*d*, Ca-*d*, Ca-*p* states. The small peak near 0.9 eV is due to the intra band transitions and is more intense when compared to 6.25% La doping because of increase in concentration of La. Refractive index is also plotted as shown in Fig. 16. The static refractive index along *x*-direction is 1.98, 2.31, 2.41, while it is 1.98, 2.56, 2.8 along *z*-direction for host, 6.25%, 12.5% La-doped CaHCl respectively. This increase in the static refractive index values with the doping may find its application in high refractive index film materials for optical coatings.

4. Conclusion

The structural, electronic, optical, and vibrational studies are calculated for the alkaline-earth hydride-halides, MHX (M = Ca, Sr, Ba

and X = Cl, Br, I) using first-principles within framework of density functional theory. Since no experimental and theoretical studies are reported so far, this may serve as a reference for future studies. These compounds crystallize in PbFCl-type tetragonal structures at ambient conditions. Our theoretical calculations exactly reproduce the ground state properties in good agreement with the experimental results. All the compounds are found to be insulators and possess optical isotropy though being structurally anisotropic. Doping on the Ca site with La has changed the electronic structure properties drastically and insulator to metal transition has been observed, and Fermi surface calculations are the evidence for the same. A quasi-two-dimensional nature evolves from the Fermi surfaces. The optical properties as a function of doping report the possible applications in the visible region of the electromagnetic spectra. The main highlights of the present work are the insulator to metal transition along with the quasi-two-dimensional which might fetch device applications.

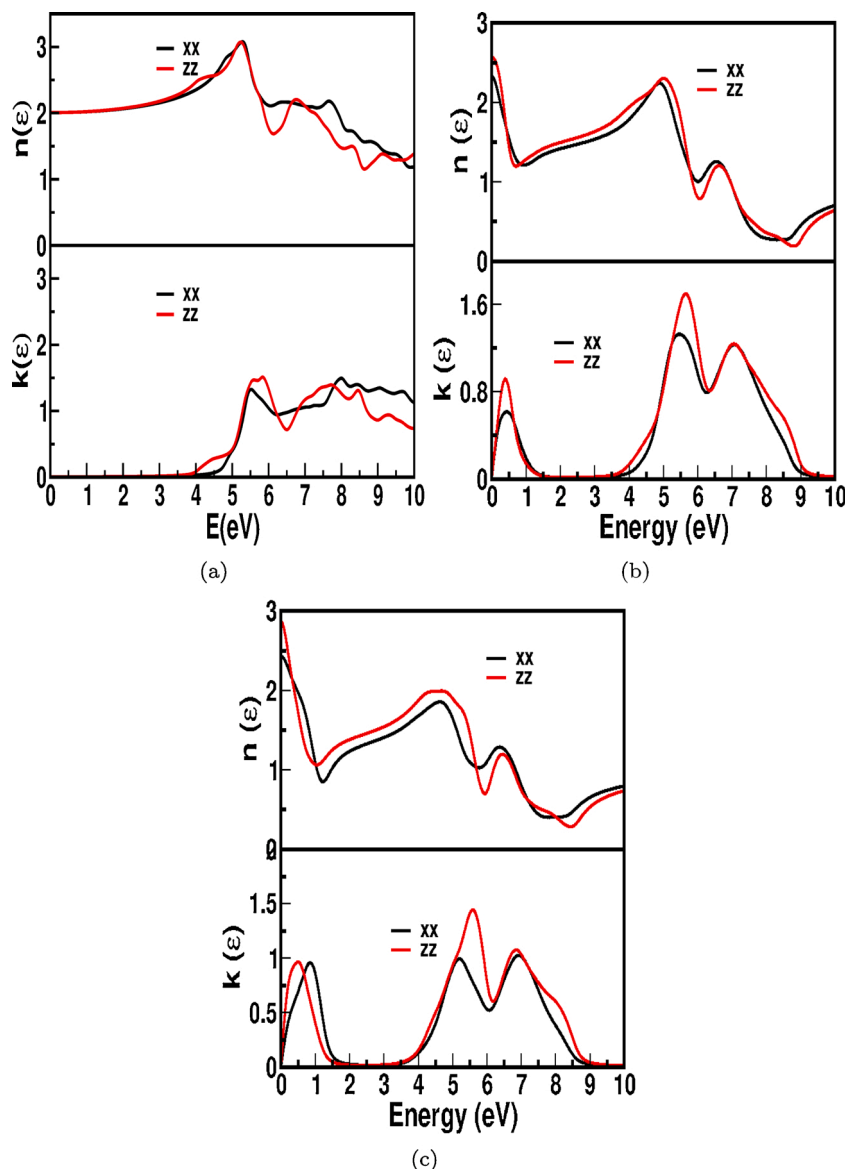


Fig. 16. Refractive index plots of (a) host, (b) 6.25% La doped, (c) 12.5% La doped CaHCl indicating the increase in the static refractive index values and decrease in the optical isotropy.

Authors' contribution

Behatha Anuroopa: executing the problem, running the calculations, data analysis, manuscript preparation. Vineet Kumar Sharma: analysis of results, editing the manuscript, discussions. Gummula Shwetha: running a part of the program, discussion of results, analysis, manuscript editing. VK: problem identification, data analysis, discussion of results, manuscript preparation and editing.

Conflict of interest

None declared.

Declaration of Competing Interest

The authors report no declarations of interest.

Acknowledgement

Authors BA, VKS would like to acknowledge IIT Hyderabad for providing computational facilities. GS would like to acknowledge IGCAR-Kalpakkam for computational facilities and fellowship. VK would like to acknowledge to CSIR project with sanction no. 03(1433)/18/EMRII. BA would like to acknowledge DST-INSPIRE for fellowship. VKS would like to acknowledge MHRD for fellowship.

Appendix A. Supplementary data

Supplementary data associated with this article can be found, in the online version, at <https://doi.org/10.1016/j.mtcomm.2020.101830>.

References

- [1] F. Hulliger, *Structural Chemistry of Layer-Type Phases*, Reidel, Dordrecht, 1975, p. 258.

- [2] R.W.G. Wyckoff, *Crystal Structures*, Wiley, New York, 1963.
- [3] G. Knoll, *Radiation Detection and Measurement*, 3rd ed., Wiley, New York, 2000.
- [4] M. Sonoda, M. Takano, J. Miyahara, H. Kato, Computed radiography utilizing scanning laser stimulated luminescence, *Radiology* 148 (1983) 833.
- [5] K. Takahashi, K. Kohda, J. Miyahara, Y. Kanemitsu, K. Amitani, S. Shinoya, Mechanism of photostimulated luminescence in BaFX:Eu²⁺ (X=Cl,Br) phosphors, *J. Lumin.* 266 (1984), 31/32.
- [6] K. Takahashi, Y. Shibahara, J. Miyahara, Photostimulated luminescence (PSL) and color centers in BaFX:Eu²⁺(X=Cl, Br, I) phosphors, *J. Electrochem. Soc.* 132 (1985) 1492.
- [7] A.R. Lakshmanan, K. Govinda Rajan, Phonon vibrational frequencies and elastic properties of solid SrFCl. An ab initio study, *Radiat. Prot. Dosim.* 55 (1994) 247.
- [8] K. Govinda Rajan, M. Yousuf, N. Subramanian, R. Kesavamoorthy, A. R. Lakshmanan (Eds.), *Photostimulated Luminescence and its Applications*, Allied Publishers, New Delhi, 1996.
- [9] N. Subramanian, R. Kesavamoorthy, V. Rajan, M. Yousuf, S. Bera, S.V. Narasimhan, X-ray excited optical luminescence, photoluminescence, photostimulated luminescence and X-ray photoemission spectroscopy studies on BaFBr:Eu, *J. Phys.: Condens. Matter* 9 (1997) 4769.
- [10] L.H. Brixner, J.D. Bierlein, V. Jhonson, in: E. Kaldis (Ed.), *Current Topics in Material Science* 4, North-Holland, Amsterdam, 1980.
- [11] U.S. Patents 4,239,968 and 4,236,078.
- [12] B. Sundarakkannan, R. Kesavamoorthy, J.A. Nisha, V. Sridharan, T. Sivakumar, Antiferroelectric-to-paraelectric transition in BaFCl, *Phys. Rev. B* 57 (1998) 11632.
- [13] N. Subramanian, N.V. Chandrashekar, P.C. Sahu, M. Yousuf, K.G. Rajan, Crystal structure of the high-pressure phase of BaFCl, *Phys. Rev. B* 58 (1998) R555.
- [14] F. Decremps, M. Fischer, A. Polian, J.P. Itie, M. Sieskind, Ionic layered PbFCl-type compounds under high pressure, *Phys. Rev. B* 59 (1999) 4011.
- [15] G. Kalpana, B. Palanivel, I.B. Banu, M. Shameem, Rajagopalan, Structural and electronic properties of alkaline-earth fluorohalides under pressure, *Phys. Rev. B* 56 (1997) 3532.
- [16] V.D. Anna, L.M.L. Daku, H. Hagemann, F. Kubel, Ionic layered BaFCl and Ba_{1-x}Sr_xFCl compounds: physical and chemical-pressure effects, *Phys. Rev. B* 82 (2010) 024108.
- [17] K. Jiang, X. Xiao, L. Chen, L. Han, S. Li, H. Ge, Q. Wang, A comparative study of the hydrogen storage properties of LiBH₄ doping with CaHCl and CaH₂, *J. Alloys Compds.* 539 (2012) 103–107.
- [18] M.V. Sofianos, S. Randall, M. Paskevicius, K.-F. Aguey-Zinsou, M.R. Rowles, T. D. Humphries, C.E. Buckley, Exploring halide destabilised calcium hydride as a high-temperature thermal battery, *J. Alloys Compds.* 819 (2020) 153340.
- [19] C. Cazorla, A.K. Sagotra, High-pressure phase diagram and superionicity of alkaline earth metal difluorides, *J. Phys. Chem. C* 122 (2018) 1267–1279.
- [20] B. Khan, H.A.R. Aliabad, N. Razghandi, M. Maqbool, S.J. Asadabadi, I. Ahmad, Structural and thermoelectric properties of pure and La, Y doped HoMn₃ for their use as alternative energy materials, *Comput. Phys. Commun.* 187 (2015) 1–7.
- [21] Y. Fang, T. Xu, Y. Zhang, X. Kong, J. Liu, S. Cui, D. Wang, Structural, electronic and optical properties of La, C-doped TiO₂ investigated by first principle calculations, *J. Phys. Chem. Solids* 132 (2019) 121–129.
- [22] M. Imada, A. Fujimori, Y. Tokura, Metal-insulator transitions, *Rev. Mod. Phys.* 70 (1998) 1039.
- [23] N.F. MOTT, *Rev. Mod. Phys.* 40 (1968) 677.
- [24] S. Doniach, Insulator-metal transition, *Adv. Phys.* 18 (1969) 81948.
- [25] N.F. Mott, *Metal-Insulator Transitions*, Taylor and Francis, London, 1974, 278 pp.
- [26] L.L. Van Zandt, J.M. Honig, Theories pertaining to the semiconductor-metal transition in crystals, *Annu. Rev. Mater. Sci.* 4 (1974) 191220.
- [27] R.F. Milligan, G.A. Thomas, The metal-insulator transition, *Annu. Rev. Phys. Chem.* 36 (1985) 13958.
- [28] N.F. Mott, *Metal-Insulator Transitions*, Taylor and Francis, London, 1990, 286 pp.
- [29] F. Gebhard, *The Mott Metal-Insulator Transition: Models and Methods*, Springer, Berlin/London, 1997, 317 pp.
- [30] P.P. Edwards, R.L. Johnston, F. Hensel, C.N.R. Rao, D.P. Tunstall, A perspective on the metal-nonmetal transition, *Solid State Phys. Adv. Res. Appl.* 52 (1999) 229338.
- [31] S.V. Kravchenko, M.P. Sarachik, Metal-insulator transition in two-dimensional electron systems, *Rep. Prog. Phys.* 67 (2004) 144.
- [32] P. Yoo, P. Liao, *Mol. Syst. Des. Eng.* 3 (2018) 264–274.
- [33] P. Yoo, P. Liao, First principles study on hydrogen doping induced metal-to-insulator transition in rare earth nickelates RNiO₃ (R = Pr, Nd, Sm, Eu, Gd, Tb, Dy, Yb), *Phys. Chem. Chem. Phys.* 22 (2020) 6888–6895.
- [34] Y. Shinohara, S. Sharma, J.K. Dewhurst, S. Shallcross, N.N. Lathiotakis, E.K. U. Gross, Doping induced metal-insulator phase transition in NiO—a reduced density matrix functional theory perspective, *N. J. Phys.* 17 (2015) 093038.
- [35] Y. Xu, Y. Sheng, Y.-f. Yang, Quasi-two-dimensional Fermi surfaces and unitary spin-triplet pairing in the heavy fermion superconductor UTe₂, *Phys. Rev. Lett.* 123 (2019) 21700217.
- [36] M.C. Payne, M.P. Teter, D.C. Allan, T.A. Arias, J.D. Joannopoulos, Iterative minimization techniques for ab initio total-energy calculations: molecular dynamics and conjugate gradients, *Rev. Mod. Phys.* 64 (4) (1992) 1045–1097, <https://doi.org/10.1103/revmodphys.64.1045>.
- [37] M.D. Segall, P.J.D. Lindan, M.J. Probert, C.J. Pickard, P.J. Hasnip, S.J. Clark, M. C. Payne, First-principles simulation: ideas, illustrations and the CASTEP code, *J. Phys.: Condens. Matter* 14 (2002) 2717–2744.
- [38] P. Blaha, K. Schwarz, P. Sorantin, S.B. Trickey, Full-potential, linearized augmented plane wave programs for crystalline systems, *Comput. Phys. Commun.* 59 (1990) 399–415.
- [39] F. Ortmann, F. Bechsted, W.G. Schmidt, Semiempirical van der Waals correction to the density functional description of solids and molecular structures, *Phys. Rev. B* 73 (2006) 205101.
- [40] A. Tkatchenko, M. Scheffler, accurate molecular van der Waals interactions from ground-state electron density and free-atom reference data, *Phys. Rev. Lett.* 102 (2009) 073005.
- [41] S. Grimme, Semiempirical GGA-type density functional constructed with a long-range dispersion correction, *J. Comput. Chem.* 27 (2006) 1787, <https://doi.org/10.1002/jcc.20495>.
- [42] S. Grimme, Accurate description of van der Waals complexes by density functional theory including empirical corrections, *J. Comput. Chem.* 25 (2004) 1463.
- [43] T. Bucko, J. Hafner, S. Lebeguer, J.G. Angyan, Improved description of the structure of molecular and layered crystals: ab initio DFT calculations with van der Waals corrections, *J. Phys. Chem. A* 114 (2010) 11814–11824, <https://doi.org/10.1021/jp106469x>.
- [44] K. Rapcewicz, N.W. Ashcroft, Fluctuation attraction in condensed matter: A nonlocal functional approach, *Phys. Rev. B* 44 (1991) 4032.
- [45] H. Ding, K.G. Ray, V. Ozolins, M. Asta, Structural and vibrational properties of α -MoO₃ from van der Waals corrected density functional theory calculations, *Phys. Rev. B* 85 (2012) 012104.
- [46] N. Troullier, J.L. Martins, Efficient pseudopotentials for plane-wave calculations, *Phys. Rev. B* 43 (1991) 1993, <https://doi.org/10.1103/PhysRevB.43.1993>.
- [47] H.J. Monkhorst, J.D. Pack, Special points for Brillouin-zone integrations, *Phys. Rev. B* 13 (1976) 5188–5192.
- [48] T. Fischer, J. Almlof, general methods for geometry and wave function optimization, *J. Phys. Chem.* 96 (1992) 9768–9774.
- [49] G. Kresse, J. Hafner, Ab initio molecular dynamics for liquid metals, *Phys. Rev. B* 47 (1993) 558.
- [50] G. Kresse, J. Furthmüller, Efficiency of ab-initio total energy calculations for metals and semiconductors using a plane-wave basis set, *Comput. Mater. Sci.* 6 (1996) 15–50, [https://doi.org/10.1016/0927-0256\(96\)00008-0](https://doi.org/10.1016/0927-0256(96)00008-0).
- [51] G. Kresse, J. Furthmüller, Efficient iterative schemes for ab initio total-energy calculations using a plane-wave basis set, *Phys. Rev. B* 54 (1996) 11169.
- [52] G. Kresse, D. Joubert, From ultrasoft pseudopotentials to the projector augmented-wave method, *Phys. Rev. B* 59 (1999) 1758.
- [53] A. Togo, F. Oba, I. Tanaka, First-principles calculations of the ferroelastic transition between rutile-type and CaCl₂-type SiO₄ at high pressures, *Phys. Rev. B* 78 (2008) 134106.
- [54] J.P. Perdew, K. Burke, M. Ernzerhof, Generalized gradient approximation made simple, *Phys. Rev. Lett.* 77 (18) (1996) 3865–3868.
- [55] V. Wang, N. Xu, J.C. Liu, G. Tang, VASPKit: A Pre- and Post-Processing Program for VASP Code, 2019. arXiv:1908.08269.
- [56] G.K.H. Madsen, D. Singh, BoltzTraP. A code for calculating band-structure dependent quantities, *J. Comput. Phys. Commun.* 67 (2006) 175, <https://doi.org/10.1016/j.cpc.2006.03.007>.
- [57] T.J. Scheidtmantel, C. Ambrosch-Draxl, T. Thonhauser, J.V. Badding, J.O. Sofo, Transport coefficients from first-principles calculations, *Phys. Rev. B* 68 (2003) 125210.
- [58] L. Jodin, J. Tobola, P. Pecheur, H. Scherrer, S. Kaprzyk, Effect of substitutions and defects in half-Heusler FeVsb studied by electron transport measurements and KKR-CPA electronic structure calculations, *Phys. Rev. B* 70 (2004) 184207.
- [59] L. Chaput, P. Pecheur, J. Tobola, H. Scherrer, Transport in doped skutterudites: ab initio electronic structure calculations, *Phys. Rev. B* 72 (2005) 085126.
- [60] V.H.P. Beck, A. Limmer, Die Verfeinerung der Kristallstrukturen von CaHCl, SrHCl, BaHCl, BaHBr und BaI, *Z. Anorg. Allg. Chem.* 602 (1983) 183–190.
- [61] H. Zhang, J. Chen, G. Ren, D. Shen, Growth by Bridgman method and luminescence properties of Na:PbFCl crystal, *J. Cryst. Growth* 267 (2004) 588–591.
- [62] S. Ye, P. Wang, J. Zhong, Z. Zhang, L. Li, Luminescence properties of GdOCl:Eu³⁺ red-emitting phosphors for whitelight-emitting diodes, *Ceram. Int.* 45 (2019) 23304–23309.
- [63] S.S. Lee, C.H. Joh, S.H. Byeon, Highly enhanced blue-emission of LnOCl:Tm prepared by dehydration of Ln(OH)₂Cl:Tm (Ln = La and Gd), *Mater. Sci. Eng. B* 151 (2008) 163–168, <https://doi.org/10.1016/j.mseb.2008.06.027>.
- [64] M. Born, K. Huang, *Dynamical Theory of Crystal Lattices*, Clarendon, Oxford, 1956.
- [65] R. Hill, The Elastic Behaviour of a Crystalline Aggregate, *Proc. Phys. Soc. A* 65 (1952) 349.
- [66] V. Kanchana, Mechanical properties of Ti₃AlX (X = C, N): ab initio study, *Eur. Phys. Lett.* 87 (2009) 26006.
- [67] V. Kanchana, G. Vaitheeswaran, Y. Ma, Y. Xie, A. Svane, O. Eriksson, Density functional study of elastic and vibrational properties of the Heusler-type alloys Fe₂VAl and Fe₂VGa, *Phys. Rev. B* 80 (2009) 125108.
- [68] V. Kanchana, G. Vaitheeswaran, A. Svane, Calculated structural, elastic and electronic properties of SrCl₂, *J. Alloys Compds.* 455 (2008) 480.
- [69] P. Ravindran, L. Fast, P. Korzhavyi, B. Johansson, J. Wills, O. Eriksson, Density functional theory for calculation of elastic properties of orthorhombic crystals: application to TiSi₂, *J. Appl. Phys.* 84 (1998) 4891.
- [70] A. Liang, et al., High-pressure raman study of Fe(IO₃)₃: soft-mode behavior driven by coordination changes of iodine atoms, *J. Phys. Chem. C* 124 (2020) 21329–21337.
- [71] M. Ayadi, M. Sieskind, Crystal growth and Raman spectra of CaHCl and CaDCl, *J. Raman Spectrosc.* 18 (1987) 147–149, <https://doi.org/10.1002/jrs.1250180217>.
- [72] S. Dobrovits, B. Kim, M. Reticcioli, A. Toschi, S. Khmelevskiy, C. Franchini, Doping-induced insulator-metal transition in the Lifshitz magnetic insulator NaOsO₃, *J. Phys.: Condens. Matter.* 31 (2019) 244002.

- [73] S. Lebgue, Electronic structure and properties of the Fermi surface of the superconductor LaOFeP, *Phys. Rev. B* 75 (2007) 75, 035110.
- [74] P.C. Martin, S. Rules, Kramers–Kronig relations, and transport coefficients in charged systems, *Phys. Rev.* 161 (1) (1967) 143–155.
- [75] N. Yedukondalu, K. Ramesh Babu, Ch. Bheemalingam, D.J. Singh, G. Vaitheeswaran, V. Kanchana, Electronic structure, optical properties, and bonding in alkaline-earth halofluoride scintillators: BaClF, BaBrF, and BaIF, *Phys. Rev. B* 83 (2011) 165117.
- [76] G. Shwetha, V. Kanchana, Optical isotropy in structurally anisotropic halide scintillators: ab initio study, *Phys. Rev. B* 86 (2012) 115209.
- [77] M. Khan, W. Cao, N. Chen, Z. Usman, D. Faraz Khan, A.M. Toufiq, M. Ali Khaskheli, Influence of tungsten doping concentration on the electronic and optical properties of anatase TiO₂, *Curr Appl. Phys.* 13 (2013) 1376–1382, <https://doi.org/10.1016/j.cap.2013.04.023>.